Dynamic Light Scattering: An Efficient Method to Determine Thermal Diffusivity of Transparent Fluids

B. Kruppa
J. Straub
Lehrstuhl A für Thermodynamic, Technische Universität München, Munich, Germany

■ The method of dynamic light scattering is presented as a suitable technique for measuring thermal diffusivities of fluids in a wide range of states. Other techniques for determining thermal conductivity and diffusivity are also presented with the aim of drawing a comparison between methods. Experimental components and various optical arrangements of typical light scattering experiments are shown along with selected experimental results. The sources of error are assessed, and measurements are compared with conductivity and diffusivity data obtained by other methods.

Keywords: *thermal diffusivity, thermal conductivity, dynamic light scattering, alternative refrigerants*

INTRODUCTION

In the field of heat transfer and energy conversion, particularly in processes operating under thermodynamic cycles, a knowledge of the thermodynamic properties of the working fluid is of vital interest, not only for understanding the process itself but also planning and designing appropriate components. Water, the primary working fluid for energy processes, has been investigated sufficiently with respect to its thermal, caloric, and transport properties.

The situation differs, however, when investigating low- and intermediate-temperature cyclic processes such as the organic Rankine cycle, heat pumps, and refrigeration processes. Here there is still a lack of thermophysical data for the appropriate fluids, particularly in the area of transport properties. This is due to the fact that transport properties such as thermal conductivity, diffusivity, and viscosity are generally difficult to measure and are burdened with uncertainties that are typically an order of magnitude greater than their corresponding equilibrium properties (such as p, ϱ, T measurements). This is shown quite clearly in the current search for environmentally acceptable substitutes for the chlorofluorocarbons typically used in those processes, which are responsible for the depletion of the stratospheric ozone layer. Although, after some four years of research, the equilibrium p, ϱ, T properties of the most promising alternatives, CH_2FCF_3 (R134a) and $CHCl_2CF_3$ (R123), have been investigated to an extent comparable to that of water, the amount of reliable measurement data on transport properties is far less and not nearly as evenly distributed, with measurements totally lacking for some states.

For calculations involving heat transfer, knowledge of the transport properties is necessary for designing and dimensioning components, as these properties appear often in the dimensionless Nusselt, Reynolds, Prandtl, Grashof, and Rayleigh numbers.

In this paper we present the technique of dynamic light scattering as an efficient means for determining the thermal diffusivity a of transparent fluids with the aim of drawing a comparison with other typical methods of determining thermal conductivity λ and diffusivity a. Using the relationship $a = \lambda/\varrho c_p$, these properties can easily be converted, provided a good equation of state for ϱ and for c_p is available. Additionally, measurements of mass diffusivity and viscosity using dynamic light scattering are feasible and have been reported [eg, 1–3]. However, a comparison with other methods would exceed the scope of this paper, hence the limitation to the properties λ and a.

METHODS OF MEASURING THERMAL CONDUCTIVITY

The classic methods of measuring thermal conductivity create temperature gradients within the investigated fluid through local heating. The most commonly used techniques are the stationary methods of parallel plates and coaxial cylinders and the nonstationary hot-wire method. Since there is an extensive amount of literature covering both the theory and practical applications of these techniques, we will limit our discussion to the typical features, advantages, sources of error, and accuracy of each method. The references cited in this paper only represent a sampling of the available literature.

Method of Parallel Plates

Ideally, the method of parallel plates investigates the flow of heat by conduction in a fluid contained between two parallel plates kept at different temperatures. The radiative and convective modes of heat transfer are reduced to

Address correspondence to Prof. Dr.-Ing. habil J. Straub, Lehrstuhl A für Thermodynamik, Technische Universität München, Arcisstrasse 21, 8000 München 2, Germany.

Experimental Thermal and Fluid Science 1993; 6:28–38

0894-1777/93/$5.00

a minimum by an appropriate choice of experimental parameters. Figure 1 schematically shows the important aspects of a thermal conductivity cell. To avoid convection, heat generated from a cylindrical upper plate (usually copper) kept at a constant temperature T_1 is transferred through the investigated fluid to a lower plate of constant temperature T_2. The fluid distance d between the plates is usually ensured by means of glass spacers. The temperatures of the plates are measured close to the fluid layer, the accuracy of these measurements being very important for the determination of λ. The upper plate is encapsulated by a guard plate of the same material and at the same temperature, to ensure that heat is transferred only through the fluid layer. The guard plate is then surrounded by an insulation cap.

To avoid deformation of the two parallel plates at high pressures, the entire cell is often immersed in a high-pressure vessel containing the fluid, which is kept at constant temperature. The thermal conductivity can then be deduced from the stationary form of the Fourier heat equation as

$$\bar{\lambda} = \frac{\dot{Q}d}{A\,\Delta T} \tag{1}$$

where $\dot{Q}$ is the measured heat transferred between the upper and lower plates (usually measured as electric heating power), A the effective area of the upper plate, and ΔT the temperature difference across the fluid layer. $\bar{\lambda}$ denotes the integrated thermal conductivity across the fluid layer, corresponding to the arithmetic mean temperature between the two plates.

Aside from the errors accrued in measuring the variables $\dot{Q}$, A, ΔT, and d, other possible sources of error are the inclusion of radiation and convection as additional modes of heat transfer and parasitic heat flow across the boundaries of the effective area A. The error due to radiation is usually kept negligible by polishing the surfaces of the plates; however, convection constitutes a major source of error, particularly when measuring near the critical region. This is due to the strong increase in the thermal expansion coefficient α_p in this region, resulting in a large Rayleigh number. Aside from the prerequisite that the cell be situated in an accurate horizontal position, the experimentor can vary only the parameters ΔT and plate spacing d to minimize convection. Recent measurements made in the critical region of ethane [4] use temperature difference ΔT and plate spacing d as small as 1 mK and 155 μm, respectively. The presence of convection can be checked by repeating experiments with different ΔT values, a rather tedious task as reaching equilibrium under these conditions can require many hours. The errors reported in this region can become as large as 10%.

A detailed description of this method, including error analysis, has been given by Michels et al [5–7]. Typical reported errors are between 1% and 5%, although comparative measurements by different authors can vary by more than this amount. Aside from the limitations imposed by the critical region, this method can be applied in a very wide range of states, with pressure and temperature resistance of the apparatus being the main limiting factors. Measurements have been made as low as 5 K with ^{4}He [8] to over 500 K [9] and with pressures as high as 300 MPa [10].

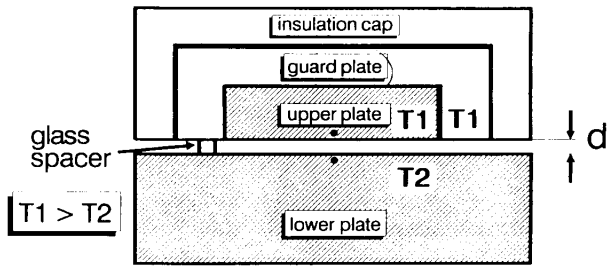

Figure 1. Method of parallel plates.

Method of Coaxial Cylinders

The principle of the method of coaxial cylinders is identical to that of the parallel-plates method. The surfaces used for heat transfer are in this case cylindrical, the inner cylinder being kept at a slightly higher temperature than the outer cylinder. The cylinders are usually mounted in a vertical position with guard heaters at either end. As with the method of parallel plates, the entire apparatus can be installed in a pressure vessel [11] or the fluid can be contained within both cylinders [12].

The sources of error are also similar; here convection poses a more serious source of error as it may occur at low Grashof numbers [13], particularly in the critical region. Since the spacing between the cylinders is kept constant (a variation of d not being practical), the only value the experimenter can control to inhibit convection is the temperature difference ΔT.

In general, the reported errors of this method are somewhat larger than those made with the parallel-plates method, particularly near the critical region. Errors of around 2% [14, 15] to over 5% [11] are typical, the critical region usually being excluded from investigation. The range of states that can be investigated is similar to that of the parallel-plates method.

Transient Hot-Wire Method

The transient hot-wire method has been developed to perfection in the last 15 years, owing in large part to the development of very fast and precise voltage-measuring devices, and has thus become a very popular and exact means for determining thermal conductivity. The apparatus can be built in a compact manner and has been fully automated [16], thus being suitable for employment in industrial applications at a relatively marginal cost in accuracy.

Figure 2 schematically demonstrates the principle of the transient hot-wire method. A very thin platinum wire, typically 7–30 μm in diameter, idealized as an infinite line source and positioned in the axis of a cylindrical cell, is surrounded by the investigated fluid kept at constant temperature. A step voltage is then applied to the wire at time $t = 0$, initiating an essentially constant heat flux $\dot{q}$. Using the wire as a resistance thermometer, the temperature of the previously calibrated wire is then successively measured as the change in resistance. The axially symmetric temperature field created around the wire is a solution of the transient Fourier equation for a cylindrical

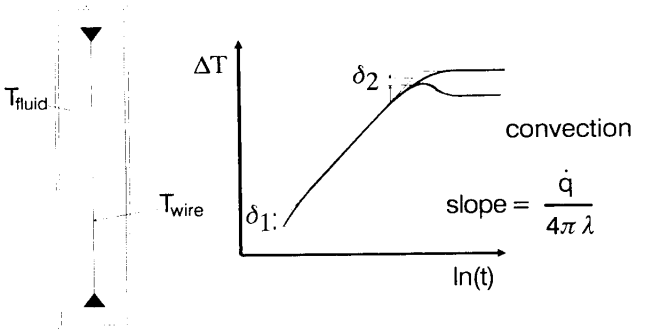

Figure 2. Schematic diagram of the hot-wire method.

configuration,

$$\varrho c_p \frac{\partial T}{\partial t} = \frac{1}{r}\frac{\partial}{\partial r}\left(\lambda r \frac{\partial T}{\partial r}\right) \qquad (2)$$

An exact solution to this equation is given in Ref. 17. The temporal behavior of the temperature increase $\Delta T = T_{wire} - T_{fluid}$ at the radial distance corresponding to the radius of wire r_w can, to a very good approximation, be given by

$$\Delta T(r_w, t) = (\dot{q}/4\pi\lambda)\ln(4at/r_w^2 C) \qquad (3)$$

where a denotes the thermal diffusivity and $C = \exp\gamma = 1.781\ldots,\gamma$ being Euler's constant. This behavior is linear (dashed line) when plotted along a logarithmic time scale (Fig. 2). The slope of this line is inversely proportional to the thermal conductivity and can be determined by fitting a straight line by a least squares method through the appropriate data points. An evaluation of the curve itself additionally yields the thermal diffusivity a of the fluid. However, a cannot be determined as accurately as λ by this method [18], which is why the values of thermal diffusivity obtained by hot-wire methods are rarely published. A comprehensive treatment of the theory and a detailed error analysis are given in Refs. 18–20.

Although there are many imperfections to this model, it can be shown that only three sources of error need be taken into account. These are a correction δ_1 due to the finite heat capacity of the wire, which appears as a deviation from the straight line at the onset of the measurements; the effect δ_2 of the finite cell dimensions (resulting in the eventual flattening of the curve); and a correction for the bath temperature (Knudsen effects) for gases at low densities. As with the stationary methods, convection poses a severe limitation because the temperature jump at the hot wire invariably gives rise to convection currents. The advantage of this method is that any convection immediately manifests itself as a deviation from the straight line (Fig. 2) and can effectively be singled out from the possible sources of error. Therefore measurement durations are very short, typically under 1 s, and the measurement has to be completed before convection becomes noticeable. This technique, however, fails in the immediate critical region, due to its transient character. Characteristics of the critical point, such as long equilibrium times, the presence of density profiles over the length of the cell, and the high susceptibility for convection require extreme experimental conditions such as measurement durations on the order of milliseconds and demand a high degree of experimental expertise. A comparison of thermal conductivity of ethane in the critical region with the method of parallel plates made by Mostert et al [4] reveals that differences in the measurements are already significant at a distance of 7 K from the critical point.

Measurements cover a wide range of states, ranging from the dilute gas region up to temperatures of 1000 K and pressures of 250 MPa with typical measurement errors reported of between 1 and 2% [eg, 21–26].

This technique can also be used as a stationary method for measuring thermal conductivity. The uncertainties, however, are greater than those in the parallel-plate and coaxial cylinder methods, typically on the order of 10%.

DYNAMIC LIGHT SCATTERING

In contrast, dynamic light scattering represents a noninvasive optical technique. The fluid under investigation is in a state of thermal equilibrium with no internal source of heat or macroscopic temperature gradients present, thus avoiding convective effects and reducing equilibration times. Information on transport properties is obtained by investigating the relaxation behavior of microscopic thermodynamic fluctuations. As the method is intrinsically absolute in nature, there is no need for calibration or for the introduction of corrective terms. The technique is applicable over a relatively wide range of states and is particularly suitable for precise measurements in the critical region. It is, however, dependent on the intensity of light scattered by the molecular fluctuations. At lower fluid densities (typically below 100 kg/m^3), the scattered intensities are too low to be evaluated accurately and thus limit the range of application. Also, as this is an optical technique, measurements are restricted to optically transparent fluids.

Theory of Dynamic Light Scattering

Since the theoretical considerations involving dynamic light scattering are rather extensive, only a simplified form will be presented here. Readers are referred to such standard literature as Berne and Pecora [27], Pecora [28], Cummins and Pike [29], and Chu [30] for more detailed information.

The technique is based on the fluctuation theory for gases and liquids first introduced by Smoluchowski [31] and Einstein [32] early in this century, which states that the molecules in fluids are constantly undergoing Brownian motion even in systems in macroscopic equilibrium. Measuring macroscopic equilibrium values is actually a process of averaging the microscopically fluctuating quantities over the fluid volume with respect to time and position. The fluctuations arising from molecular translation represent local spontaneous density fluctuations $\Delta\varrho(\mathbf{r}, t)$ about equilibrium values and can be expressed as

$$\varrho(\mathbf{r}, t) = \varrho_0 + \Delta\varrho(\mathbf{r}, t) \qquad (4)$$

where ϱ_0 denotes the macroscopically constant density. Assuming that these fluctuations are small in magnitude, the linearized hydrodynamic equations of motion can be applied to describe the behavior of the density fluctuations, which can be separated into two independent types of processes, mechanical and thermal. Both are essentially

dissipative processes and represent pressure fluctuations at constant entropy and local entropy fluctuations at constant pressure.

$$\Delta\varrho(\mathbf{r},t) = \left(\frac{\partial\varrho}{\partial p}\right)_s \Delta p(\mathbf{r},t) + \left(\frac{\partial\varrho}{\partial s}\right)_p \Delta s(\mathbf{r},t) \quad (5)$$

While the abiabatic pressure fluctuations are caused by damped sound waves traveling through the fluid, the variations in entropy are essentially due to dissipative temperature fluctuations. According to the theory of microscopic reversibility stated by Onsager [33], the laws governing the dissipative processes that dampen these microscopic fluctuations are, when averaged over a large number of cases, identical to those laws governing the appropriate macroscopic process. Therefore, macroscopic properties such as thermal diffusivity, diffusion coefficients (in mixtures), speed of sound, and sound diffusion coefficient can be obtained by investigating the temporal behavior of such molecular fluctuations. In our case the temperature fluctuations ΔT are governed by the Fourier law of heat conduction,

$$\frac{\partial}{\partial t}\Delta T(\mathbf{r},t) = a\nabla^2[\Delta T(\mathbf{r},t)] \quad (6)$$

which is exponentially decaying in its temporal behavior.

To enable the measurement of microscopic fluctuations, elastic light scattering is employed. The interaction of incident monochromatic light (laser) with the molecules creates individual oscillating dipoles that emit light in all directions at essentially the same frequency. The superposition of density fluctuations and therefore fluctuations in the local dielectric susceptibility χ_e causes the intensity of the scattered light to fluctuate also. Its temporal behavior therefore contains information of the local fluctuations of the various processes.

Light scattered by the local pressure fluctuations is slightly shifted in its frequency in both directions (but still considered to be elastic) by an amount $\Delta\omega$ proportional to the velocity of sound, while the light scattered by the entropy fluctuations is not shifted in frequency (ω_0). The broadening of either spectrum, as characterized by the half-widths at half-maximum Γ_p and Γ_s of the resulting Lorentzian distributions, is due to the dissipative process involved, in our case proportional to the sound absorption coefficient and thermal diffusivity, respectively (Fig. 3). While the frequency shift is attributed to Brillouin scattering, the unshifted frequency component is known as Rayleigh scattering. The scattering geometry in Rayleigh linewidth experiments is shown in Fig. 4. $\mathbf{q}$ is known as the scattering vector, with $\mathbf{q} = \mathbf{k}_i - \mathbf{k}_s$, $\mathbf{k}_i$ and $\mathbf{k}_s$ denoting

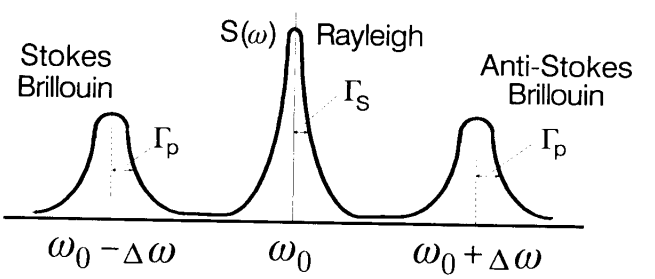

Figure 3. Frequency spectrum of elastically scattered light.

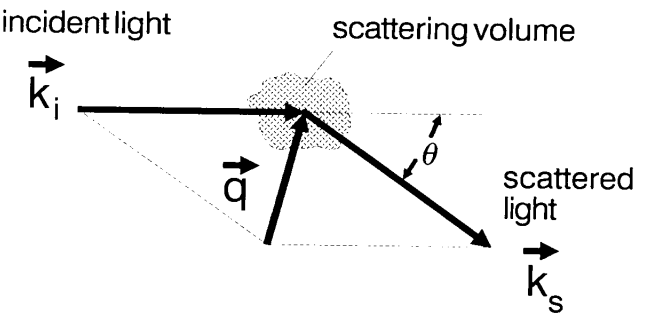

Figure 4. Scattering geometry.

the incident and scattered light vectors, respectively. $\mathbf{q}$ represents the wave component of the dielectric susceptibility fluctuations for which light is scattered in the direction $\mathbf{k}_s$. By assuming no frequency shift in the scattering process ($|\mathbf{k}_i| \approx |\mathbf{k}_s|$), we obtain

$$|\mathbf{q}| = q = \frac{4\pi n}{\lambda_L}\sin\left(\frac{\theta}{2}\right) \quad (7)$$

n, λ_L, and θ being the fluid refractive index, wavelength of light, and scattering angle in the plane set up by the wavevectors. It can be shown that the solution of the differential equation (6), when transformed in the direction of the scattering vector $\mathbf{q}$ (spatial Fourier transformation and resulting integration), is a simple decaying exponential function with a characteristic decay time $\tau_c = 1/\Gamma = 1/aq^2$,

$$\tilde{\Delta}T(\mathbf{q},t) = \tilde{\Delta}T(\mathbf{q},0)\exp(-aq^2t) \quad (8)$$

The measurement of the characteristic decay time τ_c or the broadening Γ_s of the frequency spectrum of microscopic temperature fluctuations from the intensity fluctuations of scattered light is therefore a direct measure of the thermal diffusivity of the sample.

Since the fluctuations are stochastic in nature (an individual fluctuation cannot be observed), a statistical method such as correlation provides an effective means of extracting the physical information from the intensity of scattered light. The mean behavior of a large number of fluctuations is developed in the temporal autocorrelation function $G(\tau)$, which is defined as the statistical average of the product of a time-dependent variable [in this case the intensity of the scattered light $I_S(t)$] and the same variable a certain time $(t + \tau)$ later.

$$G(\tau) = \lim_{t'\to\infty}\frac{1}{T}\int_0^{t'} I_S(t)I_S(t+\tau)\,dt \quad (9)$$

If this operation is repeated for long times ($t' \to \infty$), the correlation function depends only on the adjustable delay time τ. The exact form of the correlation function is given by the physical process under investigation. In dynamic light scattering experiments that directly investigate light scattered from temperature fluctuations alone (self-beat or homodyne detection), $G(\tau)$ takes the form

$$G(\tau) = I_S^2 + I_S^2 b_1\exp(-2aq^2\tau) \quad (10)$$

EXPERIMENTAL METHODS

Dynamic light scattering experiments measuring thermal diffusivity can be classified into experiments that directly measure the intensity of the scattered light (single-beam setup, self-beat or homodyne method), and those that superimpose a second reference beam or a local oscillator with that of the scattered light (dual-beam setup or heterodyne method). Essentially, the major components used in both setups are identical; the primary difference lies in the optical detection of the light. As the signal detected at the photomultiplier is always a superposition of light scattered in the actual scattering volume with light scattered off other objects, such as the cell windows, the general form of the correlation function is the sum of two exponential functions,

$$G(\tau) = (\bar{I}_S + I_0)^2 + \bar{I}_S^2 b_1 \exp(-2aq^2\tau) + 2I_0\bar{I}_S b_2 \exp(-aq^2\tau) \quad (11)$$

where $\bar{I}_S$ is the actual scattering intensity originating from temperature fluctuations and I_0 the intensity of the local oscillator. b_1 and b_2 are experimental constants and are functions of the number of coherence areas detected by the optical system. The second expression in Eq. (11) is known as the homodyne term, while the third expression represents the heterodyne term, the rates of decay differing by a factor of 2. Since the simultaneous evaluation of two exponential functions is always a difficult task, the homodyne detection method assumes $\bar{I}_S \gg I_0$, while correspondingly heterodyne detection assumes $I_0 \gg \bar{I}_S$.

Homodyne Method

Figure 5 shows a typical experimental setup of the light scattering apparatus employing the homodyne detection method as it is used in our laboratory at the Technical University of Munich.

Frequency-stabilized (etalon) argon ion lasers have proved to be efficient sources of light in such experiments because of their high stability and output power, typical power values lying between 1 and 300 mW, depending on the investigated region. For measurements in the critical region, where lower light intensities of a few milliwatts suffice, helium-neon lasers are applicable. As the theory of light scattering assumes Gaussian statistics of the incident light, the laser beam is usually directed through a beam expander before it is focused into the scattering volume, the beam being polarized with the polarization vector perpendicular to the scattering plane. The intensity of the scattered light is then observed at the variable angle θ by means of a photomultiplier tube. Recent advances made with avalanche photodiodes, which possess a higher quantum efficiency and other advantages such as compact dimensions, also make these instruments useful for detection [34]. However, their timing resolution (~ 10 ns) is still at least one order of magnitude lower than that of a photomultiplier tube (typically a few hundred picoseconds), leading to greater dead-time effects, which increases the error made in the determination of the decay time τ_c. To reduce self-correlation effects (afterpulse and dead-time effects) in the short time domain, two photomultipliers can be used in cross-correlation, the disadvantage being a reduction of the signal due to beamsplitting.

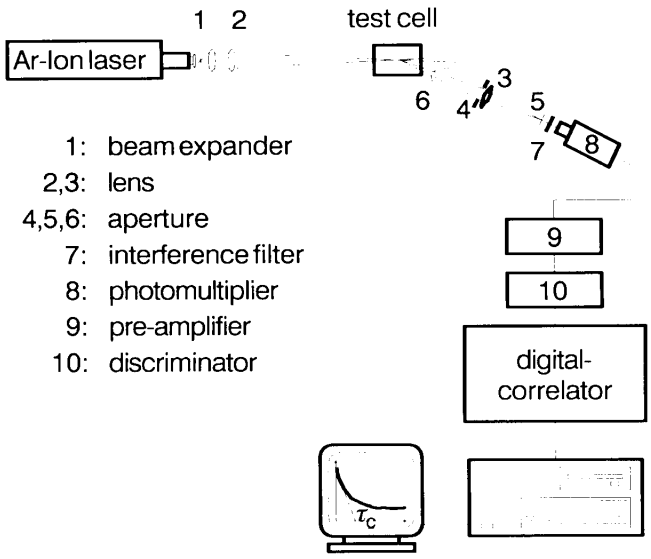

Figure 5. Schematic diagram of the homodyne detection method.

The important factor that determines the signal-to-noise ratio (S/N) and thus the detection capability of the light scattering apparatus is the amount of power scattered into a single coherence area A_{COH}. A_{COH} defines an area over which signal contributions arising from different parts of the scattering volume V are correlated and is inversely related to the dimensions of V. The laser beam should therefore be focused down to small diameters, typically < 0.1 mm. The elements of the optical system (Fig. 5), the pinhole *5*, lens *3*, and aperture *4*, determine the number of coherence areas detected by the photomultiplier and thus the light intensity as well as the angular resolution of the apparatus. These elements have to be chosen carefully, as large apertures reduce the informational content of the signal as manifested by a smaller spread of the exponential function. Although S/N itself is not influenced by these measures, the evaluation of the exponential function becomes more prone to error and run times increase substantially in this case [29, 30].

Different optical systems with varying angular, on-axis, and cross-axis resolutions can be used to project the scattering intensities generated in the scattering volume onto the surface of the photomultiplier [35]. Dual-pinhole, single-imaging-lens, or dual-imaging-lens systems are typically employed. After being amplified and passed through a discriminator, the signal if fed into a digital correlator in the form of discrete photocount events within a certain sampling interval Δt. Improvements in correlation techniques and correlator features (such as size, speed, number of channels) are continuous [36], in particular the ability of correlators to work in multiple modes with logarithmic time scales, allow for simultaneous determination of thermal diffusivity and the thermal diffusion coefficient of mixtures. The resulting photocurrent correlation function $G_i(\tau)$, a typical representation of which is shown in Fig. 6, is then usually analyzed by a nonlinear least squares fit, resulting in a direct determination of thermal diffusivity.

The homodyne method of dynamic light scattering has

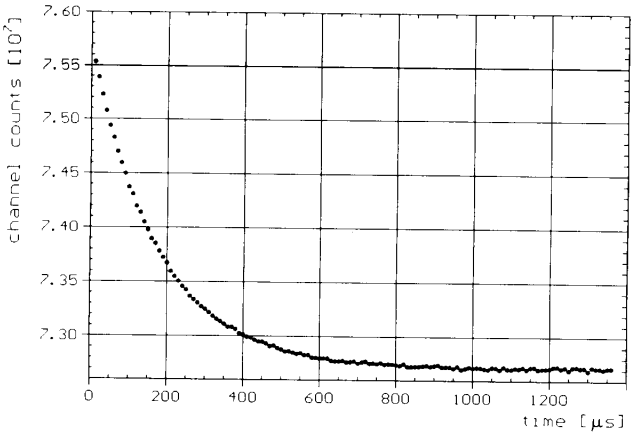

Figure 6. Typical correlation function in light scattering experiments.

often been used for measuring thermal diffusivity or diffusion coefficients near the critical point $|T - T_c| < 5$ K with scattering angles θ of 90° to avoid the superposition of light scattered from the cell windows (also known as heterodyning) [eg, 37–40]. However, with this method it is just as possible to accurately determine a and D in regions of state not usually considered critical. The primary problem is to generate sufficient scattering intensity $\bar{I}_S$ to ensure efficient correlation while keeping the assumption $\bar{I}_S \gg I_0$ valid. This can be achieved by

- Increasing the laser power
- Measuring at small scattering angles (typically 8–10°), which increases $\bar{I}_S$
- Using a single lens and pinhole imaging system with a higher on-axis resolution (at the cost of increased angular uncertainty), and
- Introducing an additional pinhole (*6*) as shown in Fig. 5 near the cell windows, which effectively screens out flare

The approximate determination of $\bar{I}_S/I_0$ can be achieved by comparing the measured intensities during a light scattering experiment with those of the evacuated cell, all other parameters being kept constant. Another possibility is a direct evaluation from the resulting coefficients of the exponential function if the geometry of the detection optics (coefficients b_1 and b_2) is known. In either case $\bar{I}_S/I_0 > 500$ in our experiments, even at distances $|T - T_c| \approx 45$ K from the critical point.

Using the described setup, we have been able to make systematic measurements of numerous substances and mixtures over a wide range of temperatures and densities typically characterized by $|T - T_c| \leq 50$ K and $0.2 \leq \varrho/\varrho_c \leq 2.5$, respectively [41–46]. As may be seen later in Fig. 8, this temperature and density range is the most interesting, with thermal diffusivity values undergoing a change of more than three orders of magnitude. At high densities thermal diffusivity is nearly constant, and it can be extrapolated to ideal gas values at low densities. Experimental run times are typically on the order of minutes for the homodyne method.

Heterodyne Method

At low fluctuation intensities, signal enhancement is achieved by superimposing a second coherent beam or local oscillator of constant intensity with the scattered light beam. While this can be done in numerous ways such as beamsplitting before and after scattering, an effective method is to include light scattered from the interior window surface in the field of view of the pinhole (Fig. 7). Varying the intensity of the local oscillator I_0 with respect to the signal intensity $\bar{I}_S$—for example, by shifting the scattering volume closer to the window surface—ensures the assumption $I_0 \gg \bar{I}_S$, reducing Eq. (11) to a single exponential,

$$G(\tau) = (\bar{I}_S + I_0)^2 + 2I_0\bar{I}_S b_2 \exp(-aq^2\tau) \quad (12)$$

Heterodyning can be a very effective method for measuring diffusivities and diffusion coefficients at further distances from the critical point, especially in the liquid region. In those regions where intensity fluctuations are very weak, a gain in the statistical accuracy of an order of magnitude can be achieved [47]. Heterodyning, however, requires coherent mixing of the scattered light and reference beam signals. The sensitivity is comparable to that of a Michelson interferometer. While the alignment problem can be circumvented by positioning the scattering volume and local oscillator source very close together, the sensitivity to intensity fluctuations in I_0 and external vibrations remains. These sources of error are difficult to avoid. Due to the weak signal $\bar{I}_S$, run times lie between 1 and 3 h.

This method has been applied in the fluid region for measuring thermal diffusivities of pure substances as well as diffusivity and diffusion coefficients of liquid mixtures [eg, 48–52].

MEASUREMENT ACCURACIES

Since dynamic light scattering represents a stochastic process, the measurements of diffusivities are invariably subject to statistical deviation. We attempt here to classify the main sources of error so as to be able to obtain an estimate of the overall accuracy of the method.

From the measurement of the decay time τ_c [Eq. (8)] and the definition of the scattering vector $\mathbf{q}$ [Eq. (7)], we obtain for the thermal diffusivity

$$a = \frac{1}{\tau_c[(4\pi n/\lambda_L)\sin(\theta/2)]^2} \quad (13)$$

Errors made in the determination of $\mathbf{q}$ can easily be assessed.

- The error made in the determination of the wavelength of incident light, λ_L, can be neglected, as the use of a frequency-stabilizing etalon reduces this error to the order of 10^{-3}%.
- Aside from its direct influence on a, errors in refractive index n also affect the determination of the scattering angle θ due to the optical geometry. However, the two errors have a compensating effect, such that a deviation $\Delta n/n$ of 10% only contributes to an error in $\Delta a/a$ of 0.3%. Thus n measurements at low scattering angles ($\theta < 10°$) need not necessarily be made. In our experiments the refractive index is

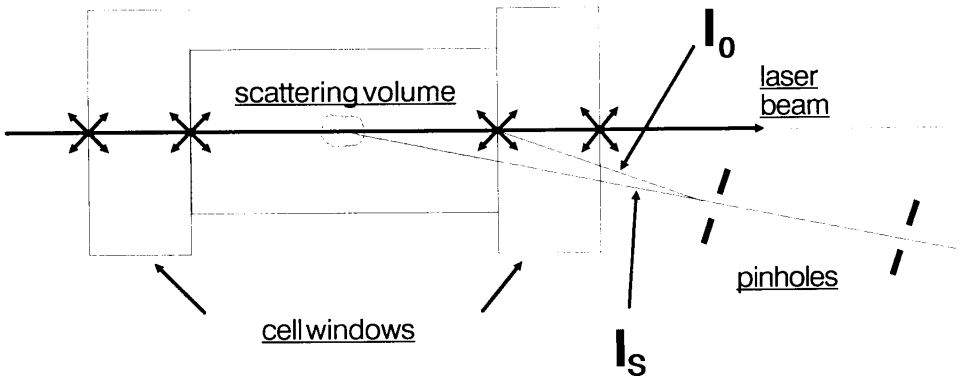

Figure 7. Optical paths of the heterodyne method.

determined with an accuracy of $\Delta n < 5 \times 10^{-4}$ by means of a prism inside the test cell. The resulting error of Δn on $\Delta a/a$ is of the order of $8 \times 10^{-2}\%$.

- The scattering angle θ must be carefully measured. In our apparatus (Fig. 5), θ is measured with an accuracy $\Delta\theta < 6''$ using a high-precision dividing head. Thus, its overall effect on $\Delta a/a < 5 \times 10^{-2}\%$ is relatively small. Measurements can also be made at different angles and along both sides of the optic axis (three on each side in our case) to further reduce errors.
- The largest source of error results from the determination of the decay time τ_c through digital correlation. As mentioned earlier, this is due to the statistical process involved. Possible error sources are listed below. A detailed investigation of statistical errors including most of the parameters listed below is given in Refs. 53 and 54.
- Afterpulse and dead-time effects of the photomultiplier become important when measuring at low light scattering intensities I_S (ie, heterodyne experiments) and high count rates (photons per unit sample time), respectively, and affect the first channels of the correlation function. Using two photomultipliers in cross-correlation practically eliminates these effects at the cost of light scattering intensity.
- Partial heterodyning or homodyning is perhaps the single largest source of error. If the assumptions $\bar{I}_S \gg I_0$ or $I_0 \gg \bar{I}_S$ are not satisfied in homodyne or heterodyne experiments, respectively, the correlation function (which is fitted to a single exponential) is contaminated by the addition of a second exponential. Calculations show that an I_0 contribution of 0.5% in homodyne experiments can account for errors in the determination of a on the order of 1% [28]. $\bar{I}_S/I_0$ can be estimated from the correlated data or obtained by experiment. With the experimental apparatus described in Fig. 5, we are able to keep the signal contribution of I_0 to under 0.2% in most cases.
- Drifts in the mean count rate for reasons unconnected with the fundamental statistical properties of the signal, arising, for instance, from suspended particles floating through the scattering volume, are a source of bias in the correlation function and have to be avoided in homodyne experiments. These effects are discussed in Ref. 53.
- Experimental parameters such as the number of coherence areas collected by the detector and the intensity of the signal at the correlator as expressed by the ratio of photon counts to coherence time can be optimized to reduce errors [29].
- The setting of the correlator sample time Δt determines the time window within which the correlation function should decay. For a correct evaluation of the exponential function, three to six decay times τ_c should be measured by the correlator.
- The finite duration of experiments introduces an error in the determination of τ_c. As the statistical accuracy of the method increases with measurement time, longer run times are desirable.

With a careful choice of experimental parameters, the errors made in the determination of τ_c can be kept within 0.5–2.0%, higher accuracies being achieved in regions of high light scattering such as the critical region.

MEASUREMENT RESULTS

In this section we present typical results measured with our apparatus described in Fig. 5. Since our objective is to systematically investigate a broad region of states around the critical point so as to be able to determine the influence of molecular properties on a, measurements are made along several sub- and supercritical isotherms (up to seven in some cases), as well as the two-phase region and along the critical isochore. In this manner, we have investigated numerous pure substances such as N_2O, SF_6, CO_2, C_2H_6, Xe, the refrigerants R13, R13B1, R22, R134a, R123, and the mixtures SF_6–CO_2 and SF_6–CHF_3 [42–46].

Figure 8 shows the results of thermal diffusivity measurements of the environmentally acceptable refrigerant R134a along six isotherms and both phases of the coexistence curve, plotted against the reduced density ϱ/ϱ_c. These measurements were made using the homodyne technique. As can be seen from the figure, all isotherms lie within the region bounded by the saturated liquid and vapor data. While measurements at higher temperatures and pressures are restricted by the pressure resistance of

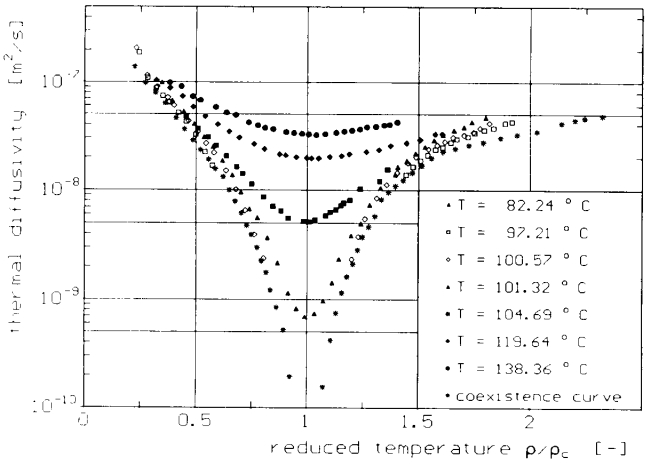

Figure 8. Thermal diffusivity of R134a along isotherms.

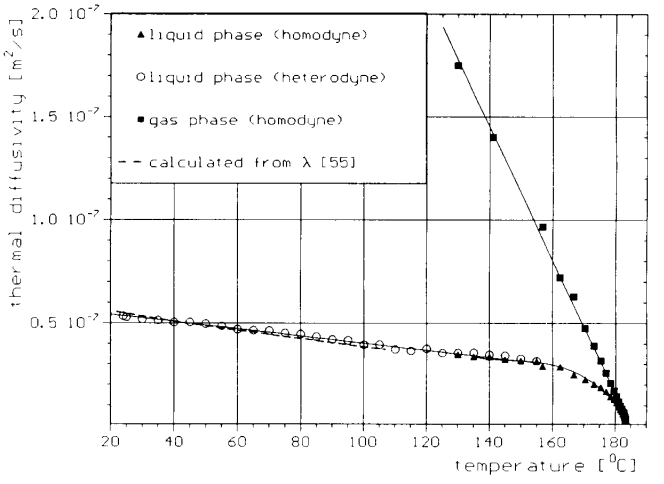

Figure 9. Thermal diffusivity of R123 in the two-phase region.

the quartz cell windows (15 MPa at moderate temperatures), those obtained in the low-density region ($\varrho/\varrho_c < 0.2$) exhibit greater scattering due to the low intensity of the scattered light signal, limiting the applicability of the method in this region.

Figure 9 depicts our new thermal diffusivity measurements of the refrigerant R123 along both phases of the coexistence curve. In the liquid phase, at temperatures below 155°C, we applied the heterodyne technique, while the other regions were measured with the homodyne technique. The region of overlap $130°C \leq T \leq 155°C$ shows good agreement between the two methods. A comparison with converted Japanese thermal conductivity measurements in the fluid region [55] also shows good agreement. As can be seen, the combination of the two techniques allows a wide range of states to be investigated.

Within the critical region, there is a strong decrease in the values of thermal diffusivities due to the strong divergence of the values of c_p, which is stronger than the increase in λ. In this region, macroscopical temperature stability becomes increasingly important, as this not only limits the possible approach to the critical point but also represents an increasing source of error in the determination of thermal diffusivity. With an electrically heated test cell (described in Ref. 56) we have been able to attain a temperature stability (over 24 h) of under 4 mK at 450 K, enabling an approach to the critical point of 0.015 K. Although the temperature stability would allow for closer approaches, other limiting factors such as cell geometry, multiple scattering effects, deviations from the hydrodynamic model, gravity effects, and effects induced by laser heating become a major source of error in this region [57].

A comparison of results of thermal diffusivity measurements with those made by the methods discussed at the beginning of this paper have often proved difficult owing to the lack of obtainable data, particularly in the critical region. Recently, however, Mostert et al [4] made accurate thermal conductivity measurements of ethane in the critical region using the method of parallel plates. The results were expressed by using an extended form of the Kawasaki equation [58] to account for the nonasymptotic critical behavior, enabling a comparison with the diffusivity data obtained by Jany and Straub [42] from light scattering experiments (Fig. 10).

The solid curves in Fig. 10 represent the calculated values of a based on the λ measurements of Ref. 4. As can be seen, the agreement is good over a broad region (including the low-density region) with deviations occurring at high densities in the fluid region.

Another method of comparison is to calculate thermal conductivity from the diffusivity data using the equation

$$a = \lambda/\varrho c_p \qquad (14)$$

Provided either an equation for the Helmoholtz free energy or an equation of state with an appropriate value of c_{p0} is available, the values of c_p and ϱ can be calculated from the T, p data. In our experiments, the values of ϱ

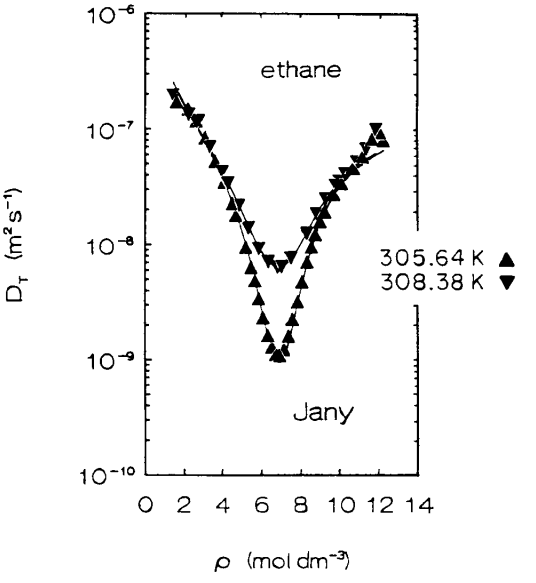

Figure 10. Comparison of thermal diffusivity of ethane. Solid line: calculated from conductivity measurements of Mostert et al [4]; symbols: diffusivity measurements from Jany and Straub [43].

are obtained by refractive index measurements, making use of the Lorentz–Lorenz relation.

Figure 11 depicts the thermal conductivity of refrigerant R22 as calculated from our thermal diffusivity data long four selected isotherms and both phases of the coexistence curve. The values of c_p were obtained by using an equation for the free Helmholtz energy developed by Marx et al [59]. Measurements obtained by Makita [14] using the method of concentric cylinders are also included. Although the agreement at distances further from the critical point is very good (90°C isotherm), large differences are observed in the critical region (100°C isotherm), the values of Makita being larger than those measured by light scattering. This is probably due to convective effects in the concentric cylinder apparatus.

The measuring methods described in the last section are based on natural statistical fluctuations within fluids. Recently, the method of forced Rayleigh light scattering has been developed by Hatakeyama et al [60] and others. Stronger, coherent temperature fluctuations are induced externally by two pulsed laser beams, which create a spatial temperature grating within the sample fluid. A probing laser of different wavelength and a photomultiplier can then be used to measure the time dependence of these fluctuations. This method has been used to measure thermal diffusivities of liquids (toluene and methanol) and liquid crystals, in some cases it being necessary to introduce a small amount of coloring substance to increase absorption.

PRACTICAL SIGNIFICANCE / USEFULNESS

Dynamic light scattering can be used as an alternative method for measuring such transport properties as thermal diffusivity, thermal conductivity, diffusion coefficients, and, if the Brillouin spectrum is evaluated, the speed of sound and the sound absorption coefficient. In comparison with other methods for measuring thermal diffusivity and conductivity, light scattering offers the distinct advantage of macroscopic thermodynamic equilibrium within the sample, which eliminates the effects of convection. Furthermore, since the evaluation involves only the decay of the exponential correlation function and not its spread or position, measurements are absolute and require no calibration. Although both the size and cost of a typical light scattering experiment have been reduced in recent years, the effort involved is still great, particularly when applying the heterodyne technique. Complete systems are commercially available; however, the actual scattering cell and its peripheral elements, such as temperature control or the introduction of a local oscillator, usually have to be individually designed and built to suit the experimental requirements.

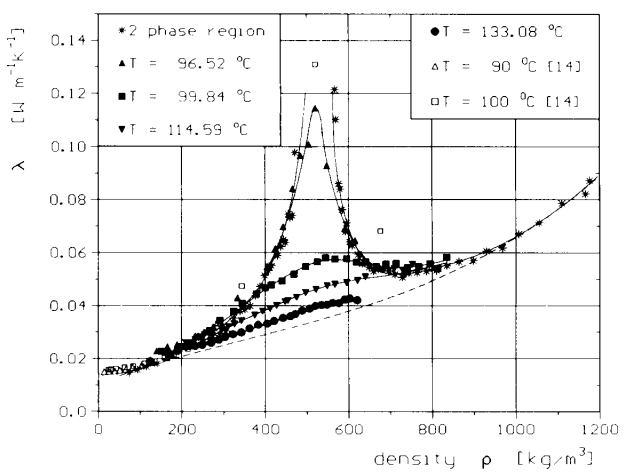

Figure 11. Comparison of the thermal conductivity of R22 by light scattering and the method of coaxial cylinders.

CONCLUSIONS

It has been shown that the method of dynamic light scattering can be used effectively for measuring the thermal diffusivity of pure fluids over a wide range of states. By combining the techniques of homodyne and heterodyne detection, measurements can be extended into the fluid region up to pressures and temperatures usually limited by constraints imposed by the experimental apparatus. In the gas region at lower densities (typically $\varrho < 100$ kg/m^3) the method of dynamic light scattering is subject to increasing errors due to low density fluctuations and resulting low scattered light intensities, and thus cannot be applied. The homodyne technique is particularly applicable in the extended critical region with typical measurement accuracies on the order of 0.5% in this area. Provided with a good equation of state for determining ϱ and c_p, thermal conductivity can be calculated from the diffusivity data. Since conventional stationary and nonstationary methods for determining λ are subject to error in the critical region due to convective effects, dynamic light scattering can be used as a complementary method to accurately determine thermal conductivities in this region.

NOMENCLATURE

A	area, m^2
A_{COH}	coherence area, m^2
a	thermal diffusivity, m^2/s
b_1	constant, dimensionless
b_2	constant, dimensionless
C	constant, dimensionless
c_p	isobaric specific heat, J/(kg · K)
D	diffusion coefficient, m^2/s
d	distance, m
$G(\tau)$	intensity correlation function
$G_i(\tau)$	photocurrent correlation function
I_S	intensity of scattered light, W/m^2
I_0	intensity of local oscillator, W/m^2
$\mathbf{k}_i$	incident scattering vector, m^{-1}
$\mathbf{k}_s$	scattered vector, m^{-1}
n	refractive index, dimensionless
p	pressure, N/m^2
$\dot{Q}$	heat flux, W
$\dot{q}$	specific heat flux, W/m^2
$\mathbf{q}$	scattering vector, m^{-1}
r	radius, m
s	entropy, J/kg
T	temperature, K
t	time, s
t'	correlation time, s
V	scattering volume, m^3

Greek Symbols

α_p thermal expansion coefficient, K^{-1}
γ Euler's constant, dimensionless
δ_1 correction term, dimensionless
δ_2 correction term, dimensionless
θ scattering angle, °
λ thermal conductivity, $W/(m \cdot K)$
λ_L wavelength of light, m
ϱ density, kg/m^3
ϱ_0 macroscopic equilibrium density, kg/m^3
τ delay time, s
τ_c exponential decay time, s
χ_e dielectric susceptibility, dimensionless
ω frequency, s^{-1}
ω_0 unshifted frequency, s^{-1}

Subscripts / Superscripts

c property of the critical point
$-$ arithmetic mean, average
$\sim$ Fourier transformed

REFERENCES

1. Saad, H., and Gulari, E., Diffusion of Liquid Hydrocarbons in Supercritical CO_2 by Photon Correlation Spectroscopy, *Ber. Bunsengen. Phys. Chem.*, **88**, 834, 1984.
2. Saad, H., and Gulari, E., Diffusion of Carbon Dioxide in Heptane, *J. Phys. Chem.*, **88**, 136, 1984.
3. Leipertz, A., Transport Properties of Transparent Liquids by Photon Correlation Spectroscopy, *Int. J. Thermophys.*, **9**, 897–910, 1988.
4. Mostert, R., Van den Berg, H. R., Van der Gulik, P. S., and Sengers, J. V., The Thermal Conductivity of Ethane in the Critical Area, *J. Chem. Phys.*, **92**, 5454, 1990.
5. Michels, A., Sengers, J. V., and Van der Gulik, P. S., The Thermal Conductivity of Carbon Dioxide in the Critical Region. I, *Physica*, **28**, 1201–1215, 1962.
6. Michels, A., Sengers, J. V., and Van der Gulik, P. S., The Thermal Conductivity of Carbon Dioxide in the Critical Region. II, *Physica*, **28**, 1216–1237, 1962.
7. Michels, A., Sengers, J. V., and Van der Gulik, P. S., The Thermal Conductivity of Carbon Dioxide in the Critical Region. III, *Physica*, **28**, 1238–1264, 1962.
8. Acton, A., and Kellner, K., The Low Temperature Thermal Conductivity of ^{4}He II, *Physica*, **103B**, 212–225, 1981.
9. Roder, H. M., and Diller, D. E., Thermal Conductivity of Gaseous and Liquid Hydrogen, *J. Chem. Phys.*, **52**(11), 5928, 1970.
10. Michels, A., and Botzen, A., A Method for the Determination of the Thermal Conductivity of Gases at High Pressures, *Physica*, **18**, 8–9, 1952.
11. Bailey, B. J., and Kellner, K., The Thermal Conductivity of Liquid and Gaseous Argon, *Physica*, **39**, 444–462, 1968.
12. Tarzimanov, A. A., and Zainullin, M. M., The Results of Measuring the Thermal Conductivity of Steam at Pressures Up to 1000 bar, *Teploenergetika*, **20**(8), 2–6, 1973.
13. Grigull, U., and Hauf, W., Natural Convection in Horizontal Cylindrical Annuli, Third International Heat Transfer Conference, Chicago, **2**, 182–195, 1966.
14. Makita, T., Tanaka, Y., Morimoto, Y., Noguchi, M., and Kubota, H., Thermal Conductivity of Gaseous Fluorocarbon Refrigerants R12, R13, R22 and R23 Under Pressure, *Int. J. Thermophys.*, **2**(3), 249–268, 1981.
15. Rosenbaum, B. M., Oshen, S., and Thodos, G., Thermal Conductivity of Argon in the Dense Gaseous and Liquid Regions, *J. Chem. Phys.*, **44**(8), 2831–2838, 1966.
16. Kawaguchi, N., Nagasaka, Y., and Nagashima, A., Fully Automated Apparatus to Measure the Thermal Conductivity of Liquids by the Transient Hot-Wire Method, *Rev. Sci. Instrum.*, **56**(9), 1788–1794, 1985.
17. Carslaw, H. S., and Jaeger, J. C., *Correlation of Heat in Solids*, 2nd ed., Oxford Univ. Press, London, 1959.
18. De Groot, J. J., Kestin, J., and Sookiazian, H., Instrument to Measure the Thermal Conductivity of Gases, *Physica*, **75**, 454–482, 1974.
19. Healy, J. J., De Groot, J. J., and Kestin, J., The Theory of the Transient Hot-Wire Method for Measuring Thermal Conductivity, *Physica*, **82C**, 392–408, 1976.
20. Kestin, J., and Wakeham, W. A., A Contribution to the Theory of the Transient Hot-Wire Technique for Thermal Conductivity Measurement, *Physica*, **92A**, 102–116, 1978.
21. De Groot, J. J., Kestin, J., Sookiazian, H., and Wakeham, W. A., The Thermal Conductivity of Four Monatomic Gases as a Function of Density Near Room Temperature, *Physica*, **92A**, 117–144, 1978.
22. Kashiwagi, H., Oishi, M., Tanaka, Y., Kubota, H., and Makita, T., Thermal Conductivity of Fourteen Liquids in the Temperature Range 298–373 K, *Int. J. Thermophys.*, **3**(2), 101–116, 1982.
23. Mardolcar, U. V., Fareleira, J. M. N. A., Nieto de Castro, C. A., and Wakeham, W. A., Measurement of the Thermal Conductivity of Argon: A Test of the Accuracy of a Transient Hot-Wire Instrument, *High Temp.–High Press.*, **17**, 469–476, 1985.
24. Roder, H. M., and Friend, D. G., Thermal Conductivity of Methane–Ethane Mixtures at Temperatures Between 140 and 330 K and at Pressures up to 70 MPa, *Int. J. Thermophys.*, **6**(6), 607–618, 1985.
25. Hahne, E., Gross, U., and Song, Y. W., The Thermal Conductivity of R115 in the Critical Region, *Int. J. Thermophys.*, **10**(3), 687–700, 1989.
26. Fareleira, J. M. N. A., Li, S. F. Y., and Wakeham, W. A., The Thermal Conductivity of Liquid Mixtures at Elevated Pressures, *Int. J. Thermophys.*, **10**(5), 1041–1052, 1989.
27. Berne, B. J., and Pecora, R., *Dynamic Light Scattering*, Wiley, New York, 1976.
28. Pecora, R., *Dynamic Light Scattering: Applications of Photon Correlation Spectroscopy*, Plenum, New York, 1985.
29. Cumminis, H. Z., and Pike, E. R., *Photon Correlation and Light Beating Spectroscopy*, Plenum, New York, 1977.
30. Chu, B., *Laser Light Scattering*, Academic, New York, 1974.
31. Smoluchowski, M., Molekular-kinetische Theorie der Opaleszenz von Gasem im kritischen Zustande, sowie einiger verwandter Erscheinungen, *Ann. Phys.*, **25**, 205–226, 1908.
32. Einstein, A., Theorie der Opaleszenz von homogenen Flüssigkeiten und Flüssigkeitsgemischen in der Nähe des kritischen Zustandes, *Ann. Phys. IV*, **33**, 1275–1298, 1910.
33. Onsager, L., Reciprocal Relations in Irreversible Processes I + II, *Phys. Rev.*, **37**, 405–426; **38**, 2265–2279, 1931.
34. Lightstone, A. W., et al., Photon Counting Modules Using RCA Silicon Avalanche Photodiodes, NASA Laser Light Scattering, Advanced Technology Development Workshop 1988, Cleveland, Ohio, pp. 65–80, September 1988.
35. Cheung, H. M., Improvement Optics for Laser Light Scattering, NASA Laser Light Scattering, Advanced Technology Development Workshop 1988, Cleveland, Ohio, pp. 119–134, September 1988.
36. Schätzel, K., Correlation Techniques in Dynamic Light Scattering, *Appl. Phys.*, **B42**, 193–213, 1987.
37. Ford, N. C., and Benedek, G. B., Observation of the Spectrum of Light Scattered From a Pure Fluid Near Its Critical Point, *Phys. Rev. Lett.*, **15**, 649–653, 1965.
38. Swinney, H. L., and Cummins, H. Z., Thermal Diffusivity of CO_2 in the Critical Region, *Phys. Rev.*, **171**, 152–160, 1968.
39. Grabner, W., Vesely, F., and Benesch, G., Rayleigh Linewidth Measurements on Polar Liquids in the Critical Region, *Phys. Rev. A*, **18**, 2307–2314, 1978.

40. Benedek, G. B., Polarisation matiere et rayonnement, in *Livre de jubile en l'honneur du Professeur Kastler*, French Phys. Soc., Eds., Presses Univ. de France, 1969.
41. Reile, E., Jany, P., and Straub, J., Messung der Temperaturleitfähigkeit reiner Fluide und binärer Gemische mit Hilfe der dynamischen Lichtstreuung, *Wärme-Stoffübertrag.*, **18**, 99–108, 1984.
42. Jany, P., and Straub, J., Thermal Diffusivity of Five Pure Fluids, *Chem. Eng. Commun.*, **57**, 67–76, 1987.
43. Jany, P., and Straub, J., Thermal Diffusivity of Fluids in a Broad Region Around the Critical Point, *Int. J. Thermophys.*, **8**(2), 165–180, 1987.
44. Kruppa, B., and Straub, J., Thermal Diffusivity of Refrigerants, in *Thermophysical Properties of Pure Substances and Mixtures for Refrigeration*, International Institute of Refrigeration, Commission BI, Eds., pp. 69–76, 1990.
45. Kruppa, B., and Straub, J., Die Temperaturleitfähigkeit von Kältemittel, DKV—Tagungsbericht 16. Jahrgang, Hannover, **2**, 383–395, 1989.
46. Kruppa, B., and Straub, J., Measurement of Thermal Diffusivity of the Refrigerants R22 and R134a by Means of Dynamic Light Scattering, Presented at the 11th Symposium on Thermophysical Properties, Boulder, Colo., Session 9.4, 1991.
47. Jakeman, E., The Effect of Heterodyne Detection on the Statistical Accuracy of Optical Linewidth Measurements, *J. Phys. A; Gen. Phys.*, **5**, L49, 1972.
48. Gulari, E., Brown, R. J., and Pings, C. J., Measurement of Mutual Diffusion Coefficients and Thermal Diffusivities by Quasi-Electric Light Scattering, *AIChE J.*, **19**, 1196–1204, 1973.
49. Czworniak, K. J., Anderson, H. C., and Pecora, R., Light Scattering Measurement and Theoretical Interpretation of Mutual Diffusion Coefficients in Binary Liquid Mixtures, *Chem. Phys.*, **11**, 451–473, 1975.
50. Krahn, W., Schwieger, G., and Lucas, K., Light Scattering Measurements of Mutual Diffusion Coefficients in Binary Liquid Mixtures, *J. Phys. Chem.*, **87**, 4515, 1983.
51. Wu, G., Fiebig, M., and Leipertz, A., Thermal Diffusivity of Transparent Liquids by Photon Correlation Spectroscopy. III. Measurements in Binary Mixtures with Large Differences in the Refractive Index of the Pure Components, *Int. J. Heat Mass Transfer*, **31**, 2555–2558, 1988.
52. Hiller, G., and Simonsohn, G., Measuring Thermal Diffusivities Using Two Photomultipliers in Cross-Correlation, in *Photon Correlation Techniques in Fluid Mechanics*, E. O. Schulz-Du-Bois, Ed., p. 377, Springer, Berlin, 1983.
53. Jakeman, E., Pike, E. R., and Swain, S., Statistical Accuracy in the Digital Autocorrelation of Photon Counting Fluctuations, *J. Phys. A, Gen. Phys.*, **4**, 517, 1971.
54. Degiorgio, V., and Lastovka, L. B., Intensity Correlation Spectroscopy, *Phys. Rev. A*, **4**, 2033, 1971.
55. *Thermophysical Properties of Environmentally Acceptable Fluorocarbons HFC 134a and HFC 123*, Japanese Association of Refrigeration, Japan, 1991.
56. Kruppa, B., Jany, P., and Straub, J., Experimental Apparatus for Measuring the Thermal Diffusivity of Pure Fluids at High Temperatures, *Int. J. Thermophys.*, **9**, 911–922, 1988.
57. Jany, P., Die Temperatureleitfähigkeit reiner Fluide im weiten Zustands-bereich um den kritischen Punkt, Ph.D. Thesis, Technische Universität München, 1986.
58. Olchowy, G. A., and Sengers, J. V., A Simplified Representation for the Thermal Conductivity of Fluids in the Critical Region, *Int. J. Thermophys.*, **10**, 417–426, 1989.
59. Marx, V., Pruss, A., and Wagner, W., Neue Zustandsgleichungen für R12, R22, R11 und R113, in *Fortschritt-Berichte 19 VDI*, VDI Verlag, Eds., **57**, 1992.
60. Hatakeyama, T., Nagasaka, Y., and Nagashima, A., Measurement of the Thermal Diffusivity of Liquids by the Forced Rayleigh Scattering Method, Thermal Engineering Joint Conference, **4**, 311–317, 1987.

Received December 17, 1991; Accepted June 30, 1992